 DOI: 10.1002/masy.201100237

3D Printing of Poly(3-hydroxybutyrate) Porous Structures Using Selective Laser Sintering

Tatiana F. Pereira,[*1] *Marcelo F. Oliveira,*[2] *Izaque A. Maia,*[2] *Jorge V. L. Silva,*[2] *Marysilvia F. Costa,*[1] *Rossana M. S. M. Thiré*[1]

Summary: Poly(3-hydroxybutyrate) (PHB) 3D porous cubes were successfully built with Selective Laser Sintering (SLS), one of the many existing 3D printing technologies. The resulting cubes presented shape and dimensions very close to the corresponding virtual model. Moreover, they were resistant to handling without presenting any visible damage. The PHB powder did not present variation in thermal properties and chemical composition after 32.15 hours of SLS process as observed by proton nuclear resonance (^{1}H NMR) and differential scanning calorimetry (DSC) analysis, indicating that it can be re-utilized to print additional structures without affecting the reproducibility of the process.

Keywords: biopolymer; poly(3-hydroxybutyrate); processing; selective laser sintering and 3D printing

Introduction

3D printing consists in slice-by-slice fabrication of three-dimensional physical objects directly from a digital model. The digital model is sliced and, each slice is than reproduced physically, successively, one on the top of other till the object is completed.[1] The slices stacking and adhesion occur concomitantly along with the slices physical definition. The 3D printing allows the manufacture of objects having complex geometries, intricate internal structure such as parts inside of parts, features with very thin walls,[1] large empty volumes and integrated movable parts.[2] Production of prototypes and functional models can be achieved in less time and at lower cost when compared with conventional process of parts fabrication.[1] These technologies also allow the confection of objects having controlled size and regular geometry pores spatially distributed within and throughout their volumes, what is not attainable by other fabrication technologies. Also, the pores can be arranged in a gradient distribution of size and shape, designing density and rigidity gradient simultaneously.[2] The capability of generating porous objects with this level of control expands the application of the 3D printing in different areas such as scaffolds for tissue engineering, filtration and also for lightweight structures for applications in implants and aerospace engineering.[2]

In Selective Laser Sintering (SLS), one of the many 3D printing technologies available, the slices are written by a CO_2 laser beam (10.6 μm wavelength) onto each of a series of powder layers deposited one on the top of the other. The written process derives from the coalescence of particles through sinterization caused by the application of laser and thermal energy.[3] The slices geometries are defined by selective sinterization that follows the laser beam scanning onto the powder layers, according to the digital slices. The heat generated by the laser beam cross the layer thickness and reaches the previously built layer promoting adherence between them. The sintered

[1] Programa de Engenharia Metalúrgica e de Materiais/COPPE, Universidade Federal do Rio de Janeiro – UFRJ, Rio de Janeiro – RJ
E-mail: tatianaf@metalmat.ufrj.br
[2] Divisão de Tecnologias Tridimensionais, Centro de Tecnologia da Informação Renato Archer, DT3D/CTI, Rod. Dom Pedro I, Km 143.6, Campinas – SP

material forms the object and the powder supports it during its manufacture.[4] In the final stage of the SLS process the object is removed from the powder environment and following it is cleaned of remained powder attached to its walls.

Powder remaining from the process (PRP) can be reused or not depending on its degradation degree, which, in turn depends on the heating undergone.

The amount of PRP powder in a typical printing process is exceedingly large (more than 85–90 per cent).[5] According to DT3D/CTI experience, 50 per cent of the initial amount of powder is discarded, in average, due to thermal decomposition. In order to minimize costs, SLS machine makers recommend, in the case of poliamide-12 that is the most commonly raw material used in SLS printing, mixing a portion of unprocessed polyamide-12 to a PRP one for additional printing. However, objects obtained with reused powder, many times irrespective of the percentage of unprocessed material, shows poorer quality compared to the objects printed only with unprocessed polyamide-12.[5]

Poly(3-hydroxybutyrate) (PHB) is a natural thermoplastic polyester produced by microorganisms under imbalanced growth conditions.[6] PHB presents mechanical properties close to those of conventional thermoplastics such as isotactic polypropylene [7] and of others biodegradable polyesters such as polylactides.[6] This polymer has attracted attention for applications in biomedical areas, as in the production of scaffolds for tissue engineering due to its biocompatibility and biodegradability. Nevertheless, only few works have been published using PHB or its copolymer as raw material in SLS processing, despite the potential of the technique for building up porous structures with very controlled pore size that are very important for cell growth support. Moreover, unlike traditional techniques such as injection molding and extrusion, PHB processing by SLS can be made without the incorporation of additives such as plasticizer.

Oliveira and collaborators[8] reported PHB porous structures successfully produced with height around 2.5 mm and pores size of 1 mm. Duan and co-workers[9] produced poly(hydroxybutyrate-co-hydroxyvalerate) (PHBV) and Ca-P(calcium phosphate)/PHBV nanocomposite scaffolds using SLS applying a experimental factorial design. The optimized scaffolds showed good structure and handling stability, with external dimension well controlled and porous structure comparable to the computational design.

In the present work PHB is employed as raw material for SLS technology. The key point is to evaluate PHB thermal stability under the process heating to determine if it can be re-used in additional printing, which is an extremely important factor for the economic feasibility of the process.

Experimental Part

Materials

The poly(3-hydroxybutyrate) (PHB) in powder form was provided by PHB Industrial S/A (Biocycle ® 1000 - lot 122, Sao Paulo, Brazil) with weight average molar mass of around 600,000 g/mol (obtained by GPC) and density of 1.22 g/cm^3, data reported by the PHB's supplier.

3D Digital Model

The CAD model of the samples was draw using SolidWorks® in the approximate shape of a cube ($L \times W \times H = 10.407 \times 10.350 \times 10.140\,mm^3$) with internal architecture composed of 16 circular pins with a diameter of 1.668 mm arranged orthogonally with 32 pins with a diameter of 1.641. These pins arrangement resulted in orthogonal channels measuring 0.836 mm in diameter (Figure 1a-b). The CAD model was saved in a STL format and loaded in the computer of the SLS equipment.

Physical Model – 3D SLS Printing

The porous cubes were printed in a Sinterstation® 2000 SLS equipment (3D System). Figure 2 shows a general scheme

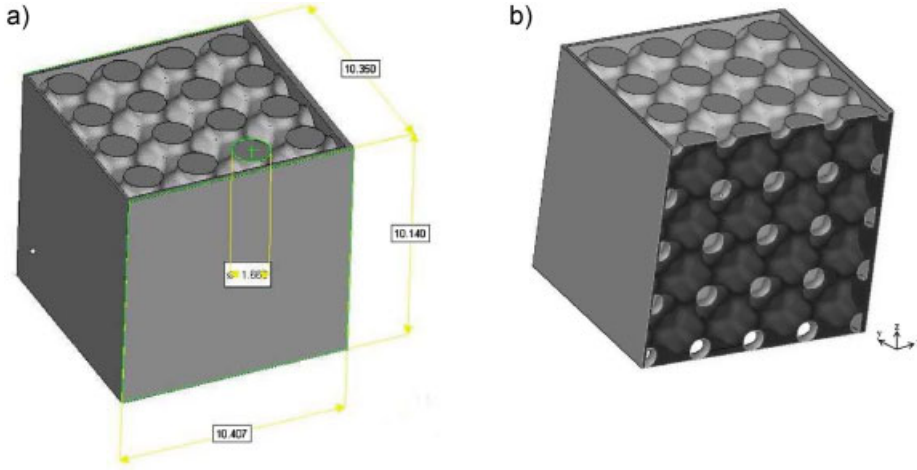

Figure 1.
Digital models of the porous cube. (a) view of the external faces and (b) view of the internal architecture.

of the SLS process. In an inert chamber, the powder layers are formed by a roller that spreads and, at the same time, compacts the powder along a platform that contains five big holes connected to containers underneath (Figure 2a). The central container (build cylinder) has a mobile bottom (construction base) that is in the platform level at the beginning of the SLS processing (Figure 2a - 9) and it is where the laser beam scanning occurs onto the powder layer. The central container is called powder bed and it contains the object in the printing process and the powder that supports it. (Figure 2a – 8). The containers situated next to both sides of the powder bed are the feeders (Figure 2a - 7). During the printing process the powder bed bottom moves downward leaving a gap that determines the thickness of the powder layer and by its turn the thickness of the object slice. Inversely the feeders bottoms move upwards elevating the powder to a position that allow it to be collected and spread by the roller (Figure 2b, e). The roller carries the powder that fills the part bed gap (whereupon a fresh powder layer) and, in its way to the edges of the platform, it carries the powder excess (not used in the gap filling) to the two remaining containers that are called overflows (Figure 2c, f). The layer powder is heated in three zones along the platform with three radiant heaters installed on a second platform situated above the powder layer platform (Figure 2a - 3). The central heater raise the part bed temperature below the sinterization point, and the laser beam provides the heating increment necessary to start the sinterization process (Figure 2d, g). The remaining two heaters heat the powder on the surface of the feeders to avoid thermal stress when it is deposited on the top of the previously sintered layer on the part bed. All types of the movement - bottoms of the part bed, feeders, roller and the laser scanning mechanism - occur synchronically and repeatedly until the object completion.

The laser parameters used for printing the cubes were: laser power (LP) = 16 W; laser scan speed (LS) = 2000 mm/s; laser beam spot = 450 μm and scan spacing (SS) = 0.15 mm.

These parameters provided a laser energy density of 0.053 J/mm^2, which was calculated according to equation described elsewhere.[10] The part bed temperature, layer thickness and roller speed were 100 °C, 0.18 mm and 127 mm/s, respectively. The removal of powder

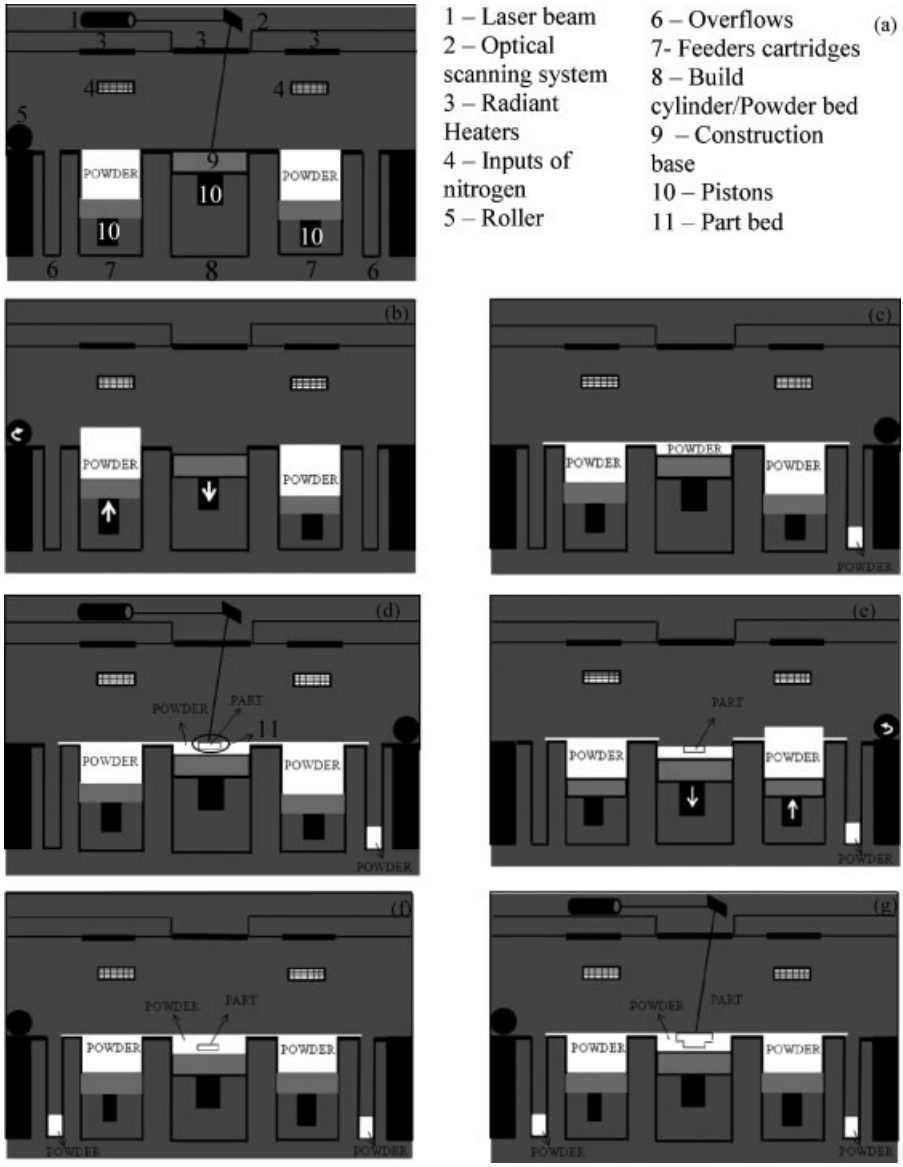

Figure 2.
Schematic of the selective laser sintering process. (a) Main components of an SLS machine (b), (c) Formation of the powder layer, (d) Laser Beam Scanning, (e), (f) Formation of the next powder layer, (g) Laser scanning of the new layer.

attached to the part was done by blowing compressed air.

The feeders were loaded with unprocessed PHB and PHB powder which underwent several printing sets. The first printing set consisted of 7 printings of 30 minutes each giving a total of 3.5 hours of SLS process, running with laser energy density (ED) varying from 0.023 to 0.083 J/mm^2. Afterwards, the powder in the machine was thoroughly removed and the feeders were loaded with the overflow powder from 1st printing set. Then a second printing set was performed which consists of 4 printings of 30 minutes each taking a total of 2 hours. The laser energy density

varied from 0.023 to 0.053 J/mm^2. In the third printing set, the feeders were loaded with PHB powder which was submitted to 30.45 hours of several SLS process cycle. The laser energy density during this set varied from 0.033 to 0.053 J/mm^2.The PHB powder from part bed after 1st printing set ('part bed powder – 3.5h') and after 3rd printing ('part bed powder – 32.15 h') was characterized as well as the parts produced in those three printing sets with ED of 0.053 J/mm^2.

Evaluation of Isothermal Thermal Degradation of PHB

To investigate the influence of processing time in the thermal degradation of PHB samples of unsintered powder were placed in an oven with controlled temperature and nitrogen rich atmosphere (vacuum oven, Marconi MR030). These samples were heated at temperature of the 140 °C and kept for 3.5, 25, 50 h. The temperature of 140 °C was chosen for this experiment because it was an intermediate value between part bed temperature (100 °C) and PHB melting temperature (about 180 °C).

Characterization

Thermal properties and degree of crystallinity of the PHB powder (unprocessed, part bed after the 1st and 3rd printing sets and powder kept at 140 °C for different times) and PHB cubes obtained in the 1st, 2nd and 3rd printing sets) were evaluated in a Perkin Elmer DSC 8000 differential scanning calorimeter. Both first and second heating cycle were carried out in the same heating conditions, from −20 °C to 210 °C, at a rate of 10 °C/min. The first cycle was followed by a rapid cooling at a rate of 150 °C/min till −20 °C. The thermal transitions and the enthalpy of fusion were obtained from DSC curves in the second heating and temperatures were taken at the peak maximum. The crystallinity degree (Xc) of the specimens was calculated using the Equation 1, where, ΔH_f is the enthalpy of fusion and ΔH_f^0 is enthalpy of fusion of 100% crystalline PHB (146 J/g).[11]

$$Xc = \left[\frac{\Delta H_f}{(\Delta H_f^0)}\right] \times 100 \quad [1]$$

Proton Nuclear Magnetic Resonance (^{1}H NMR) of the PHB powder (unprocessed and from part bed after the 1st printing sets and 3rd printing sets) was carried out in a Varian Mercury VX 300 MHz at 40 °C. The samples were dissolved in deuterated chloroform ($CDCl_3$).

The cubes from the printing sets were analyzed in terms of digital model replication, morphology (SEM) and thermal behavior (DSC). The morphologies of external and longitudinal fracture surfaces of PHB cubes were investigated using a scanning electron microscope (SEM), JEOL JSM-6460 LV. The specimens were previously coated with a thin gold layer and examined at an acceleration voltage of 15 kV. The Table 1 summarizes the printing sets and analysis scheme.

Table 1.
SLS printing scheme with PHB powder and analysis performed.

Printing reference	Powder loaded in the feeders	Printing duration	Analyses performed
1st printing set	Unprocessed powder	3.5 hours	-DSC of powder after 1st printing set (3.5 h) and physical model - ^{1}NMR of powder - SEM of physical model
2nd printing set	Overflow powder from the 1st printing (3.5 h)	2 hours	- DSC of the physical model - SEM of physical model
3rd printing set	Powder from overflow, powder bed and feeders after several printings of 30.45 h	1.5 hours	- DSC of physical model and of powder after 3rd printing set (32.15 h) - ^{1}NMR of powder

Results and Discussion

Comparison between Digital and Physical Cubes

The physical cubes showed similar geometry compared to its correspondent digital model as shown in Figure 2. The circular pins drew in the virtual model (Figure 3a) can be observed in the SEM image (Figure 3a). The cubes showed dimensional deviations with respect to the CAD model. Moreover they did not show delamination (slices detachment). In general, delamination occurs when the energy density is low, what causes poor bonding between the physical slices.[12] Thick powder layers that, by turn, produce thick slices, can also cause delamination, since the laser beam does not penetrate deeply enough in the powder layers.[9] The laser energy density ($0.053\,J/mm^2$) supplied to the material particles and layer thickness (0.18 mm) employed in this study allowed the production of a physical model without delamination.

The removal of residual PRP powder of the sample in the cleaning step was not complete, leaving trapped powder inside some channels as indicated by the circles in Figure 3b. The difficulty in removing powder attached to the walls is probably due to undesirable thermal adhesion[13] which caused the poor resolution found for pores and pins. The size of the laser spot (450 μm) compared to the sizes of these structures is a main factor that determines poor resolution.

SEM images show the presence of long necks in physical models produced in 2nd printing set that characterize the occurrence of sintering in these locations (Figure 4). However, pores that do not exist in the virtual model were also observed, suggesting incomplete particles sintering as indicated by the arrows in Figure 4b). For applications such as scaffolds for tissue engineering, the extra pores induced by SLS process are not harmful. Rather, they can be particularly useful and, in addition to the porosity already predicted in the model, can promote cell proliferation, transport of nutrients and waste removal.[13] It is worth noting that there were no significant differences in morphology of physical models from 1st, 2nd and 3rd printing sets (data not shown).

Figure 5 shows the DSC second heating curves obtained for the physical models from the 1st, 2nd and 3rd printing sets. Table 2 summarizes the thermal properties obtained. It can be observed that there was no significant variation in the temperatures of thermal transitions as well as in the degree of crystallinity between the physical models

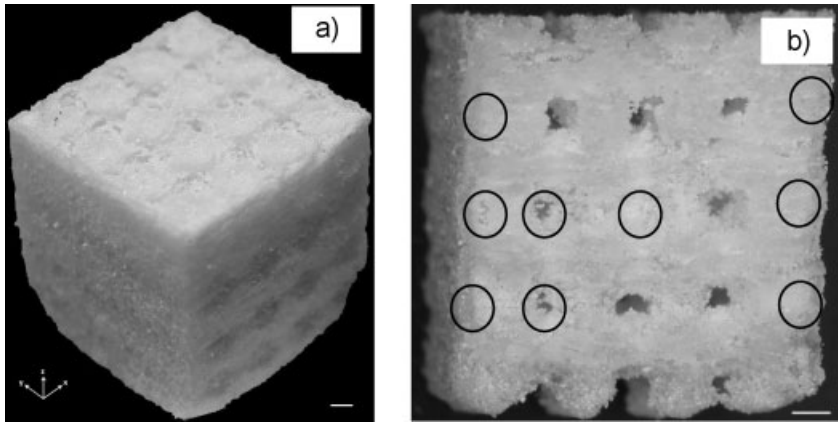

Figure 3.
Photographic images of printed PHB models of the porous cubes produced in 2nd printing set. (a) isometric view of the porous cube, (b) internal view of the porous cube (Scale bars = 1 mm).

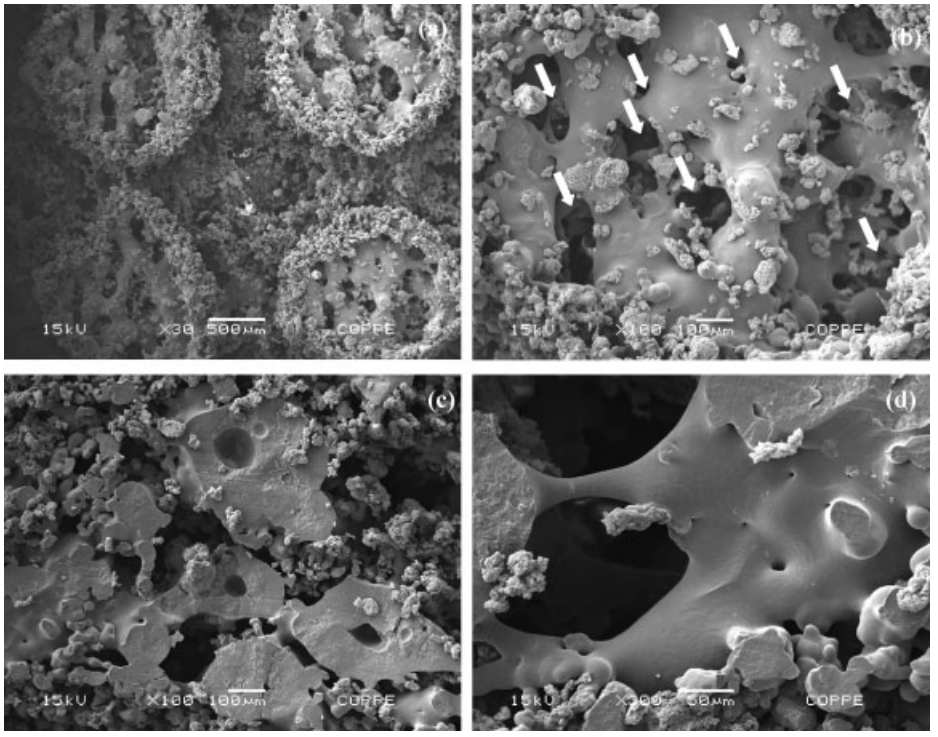

Figure 4.
SEM images of printed PHB models of the porous cubes produced in 2nd printing set. (a) and (b) top external surface, (c) and (d) longitudinal fracture (y-z plane).

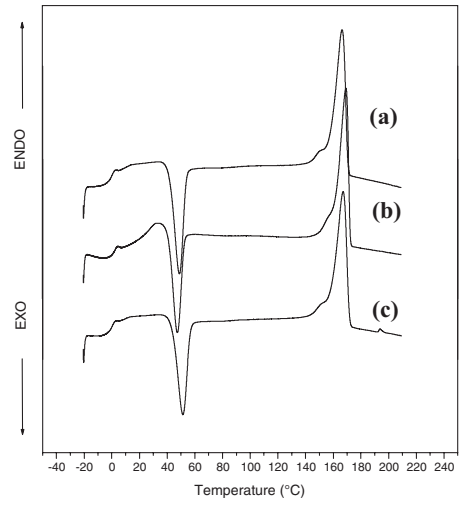

Figure 5.
DSC curves of second heating scan of physical models obtained in the 1st printing set (a), 2nd printing set (b) and 3rd printing set (c).

built in the different printing sets. These results suggested that the PHB powder did not degrades during the 32.15 hours-SLS printing and can be reused for new printing without altering the thermal properties of new cubes or any other physical models.

The re-usability of the PHB shown by the DSC analyses of the physical models is corroborated by the analysis of powder samples. Unprocessed powder and powder collected in the part bed after 1st printing set and 3rd printing set (3.5 h and 32.15-SLS printing) were compared regarding ^{1}H NMR and DSC analysis.

It is known that SLS process usually involves a complex heat transfer mechanism by radiation, convection and conduction in the feeders and in the powder bed.[14] Ariffin et al.[15] proposed that PHB undergoes thermal degradation by mainly random chain scission with subsequent auto-accelerated transesterification and a

Table 2.
Thermal properties and crystallinity degree of physical models obtained with unprocessed PHB and PHB powder which underwent of printing sets obtained by DSC curves of second heating scan.

Thermal Properties	Physical Models		
	1st printing set	2nd printing set	3rd printing set
Melting temperature, °C (Tm)	166.5	169.3	167.2
Crystallization temperature, °C (Tc)	48.9	47.3	51.3
Glass transition temperature, °C (Tg)	−0.8	1.03	−0.95
Enthalpy of fusion, J/g (ΔH_f)	77.8	78.2	76.5
Degree of Crystallinity, % (Xc)	53.0	53.5	52.0

chain reaction from crotonate chain ends. In this way, it is expected that if PHB powder was degraded during SLS process, its chain would present double bonds.

The ^{1}H NMR spectra of unprocessed PHB and part bed powder sample from 1st and 3rd printing sets were similar as can be observed in Figure 6. The part bed powder spectra did not show any peak related to hydrogen bond to an unsaturated carbon,[16] what is expected when thermal degradation of PHB due to SLS processing conditions occurs. Additionally it was observed a peak around the chemical shift of 1.55 ppm that was attributed to water dissolved (monomeric) in $CDCl_3$.[17]

Figure 7 shows the DSC curves in the second heating on the scan analysis of unprocessed PHB and part bed powder of the 3rd printing. Table 3 summarizes the thermal properties obtained from this scan. Regarding the DSC thermal analysis the part bed powder sample showed no significant changes in the transition temperatures and degree of crystallinity with respect to the unprocessed PHB (Table 3). It means that PHB powder undergoing 32.15 hours of SLS processing

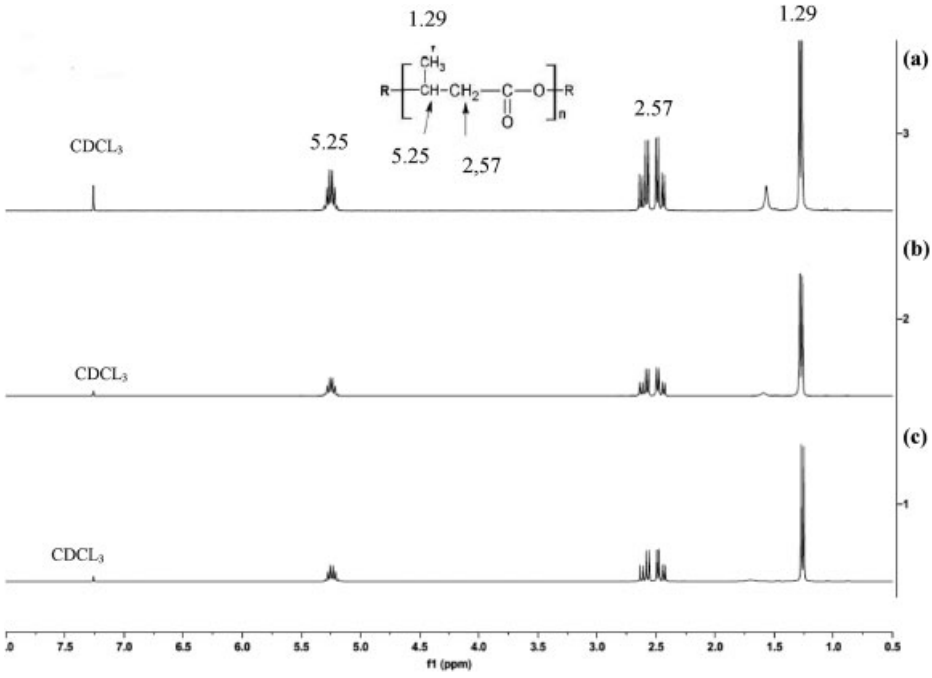

Figure 6.
^{1}H-RMN spectra (a) unprocessed PHB, (b) part bed powder – 3.5 h and (c) part bed powder – 32.15 h.

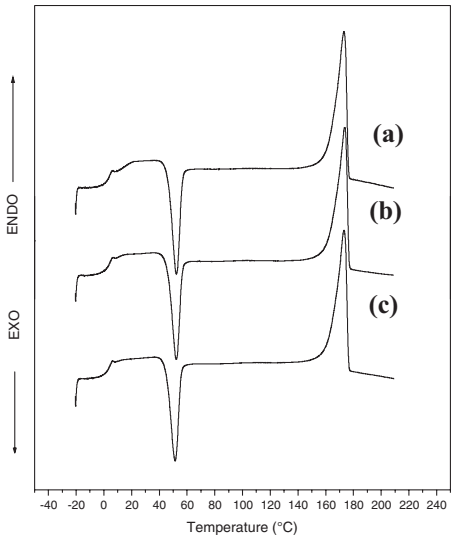

Figure 7.
DSC curves of second heating scan for unprocessed PHB (a), part bed powder of the 1st printing (b) and part bed powder of the 3rd printing (c).

preserves its thermal characteristics and, therefore, can be re-used for additional printing. Pham *et al.*[14] reported that polyamide powder (PA220) collected from building chamber and used once in the SLS process for about 20–40 h showed an increase around of 4 °C and 2 °C in glass transition temperature and melting temperature, respectively. Even with these slight changes, based in others experimental results, the authors claim that PA220 under this condition could be re-used.

Unprocessed PHB powder samples were exposed to temperature of 140 °C in an oven at nitrogen atmosphere for periods of time up to 50 h in order to simulate the deterioration of powder during SLS process in builds. The results obtained by DSC did not showed significant alterations in thermal parameters and degree of crystallinity of polymer, which corroborated the assumptions above-discussed (Table 4). It was noted that ΔH_f and Xc values decreased during 3.5–25 h, but they were recovered to original values after 50 h.

Conclusion

In this work, printing PHB three-dimensional structures were successfully produced using

Table 3.
Thermal properties and degree of crystallinity of unprocessed PHB and part bed powder of the 1st printing obtained by DSC curves of second heating scan.

Thermal Properties and degree of crystallinity	Powder samples		
	Unprocessed PHB	From 1st printing part bed – 3.5 h	From 3rd printing part bed – 32.15 h
Melting temperature, °C (Tm)	173.2	173.7	173.2
Crystallization temperature, °C (Tc)	52.3	52.2	51.4
Glass transition temperature, °C (Tg)	2.7	3.16	2.7
Enthalpy of fusion, J/g (ΔH_f)	76.9	80.14	80.7
Degree of Crystallinity, % (Xc)	53	55	55

Table 4.
Thermal properties and degree of crystallinity obtained by DSC curves of second heating scan of unprocessed PHB submitted to 140 °C for different periods of time in nitrogen atmosphere.

Thermal Properties and degree of crystallinity	Time of isothermal degradation at 140 °C			
	0 h	3.5 h	25 h	50 h
Melting temperature, °C (Tm)	173.2	173.5	173.3	173.2
Crystallization temperature, °C (Tc)	52.3	53.3	54.1	48.2
Glass transition temperature, °C (Tg)	2.7	3.18	3.51	3.23
Enthalpy of fusion, J/g (ΔH_f)	76.9	77.7	69.9	77.2
Degree of Crystallinity, % (Xc)	53	53	48	53

SLS technology. The physical models showed geometrical and dimensional features very close to the digital model. It was also demonstrated from DSC and ^{1}H NMR that the PHB powder was not altered after being submitted to 32.5 hours of SLS processing. The thermal properties of the physical model obtained with unprocessed PHB and PHB powder which underwent printing sets showed no significant difference between them. This corroborated the powder analysis that indicated that the re-use of remaining material from a 32.15-SLS did not affect the reproducibility of the process.

Acknowledgements: Authors thank the Brazilian agencies CNPq and FAPERJ for financial support and PHB Industrial S/A for supplying the PHB. Laboratory of Nuclear Magnetic Resonance of IMA/UFRJ is also thanked for NMR analysis.

[1] K. G. Cooper, in: "*Rapid Prototyping Technology: Selection and Application*", Eds., Marcel Dekker, Inc., New York **2001**, p. 1.
[2] M. F. Oliveira, I. A. Maia, P. Y. Noritomi, G. C. Nargi, J. V. L. Silva, B. M. P. Ferreira, E. A. R. Duek, in *Anais do 10° Congresso Brasileiro de Polímero, Foz do Iguaçu*, **2009**.
[3] S. Das, in: "*Virtual Prototyping & Bio Manufacturing in Medical Applications*", B., Bidanda, P. J. Bártolo, Eds., Springer, New York **2008**, p. 229.
[4] K. Senthilkumaran, P. M. Pandey, P. V. M. Rao, *Mater. Des.* **2009**, *30*, 2946.
[5] K. Dotchev, W. Yusoff, *Rapid Prototyping Journal* **2009**, *15*, 192.
[6] S. K. Misra, S. P. Valappil, I. Roy, A. R. Boccaccini, *Biomacromolecules* **2006**, *7*, 2249.
[7] K. Sudesh, H. Abe, Y. Doi, *Prog. Polym. Sci.* **2000**, *25*, 1503.
[8] M. F. Oliveira, I. A. Maia, P. Y. Noritomi, G. C. Nargi, J. V. L. Silva, B. M. P. Ferreira, E. A. R. Duek, *Revista Matéria* **2007**, *12*, 373.
[9] B. Duan, W. L. Cheung, M. Wang, *Biofabrication* **2011**, *3*, 1.
[10] J. C. Nelson, "*Selective laser sintering: a definition of the process and an empirical sintering model.*", PhD dissertation, University of Texas. Austin, TX: **1993**.
[11] M. Erceg, T. Kovačić, I. Klarić, *Polym. Degrad. Stab.* **2005**, *90*, 313.
[12] V. E. Beal, R. A. Paggi, G. V. Salmoria, A. Lago, *J. Appl. Polym. Sci.* **2009**, *113*, 2910.
[13] W. Y. Zhou, S. H. Lee, M. Wang, M. L. Cheung, W. Y. IP, *J Mater Sci: Mater Med* **2008**, *19*, 2535.
[14] D. T. Pham, K. D. Dotchev, W. A. Y. Yusoff, *Proc. Inst. Mech. Eng. C J. Mech. Eng. Sci.* **2008**, *222*, 2163.
[15] H. Ariffin, H. Nishida, Y. Shirai, M. A. Hassan, *Polym. Degrad. Stab.* **2008**, *93*, 1433.
[16] S. Nguyen, R. H. Marchessault, *Macromol. Biosci.* **2004**, *4*, 262.
[17] R. M. Silverstein, F. X. Webster, D. J. Kiemle, "*Identificação Espectrométrica de Compostos Orgânicos*", 7th Ed. LTC, Rio de Janeiro, **2006**, p. 147.

